# Journal Pre-proof

## Non-linear finite element model for dynamic analysis of high-speed valve train and coil collisions

Zewen Gu , Xiaonan Hou , Elspeth Keating , Jianqiao Ye

Please cite this article as: Zewen Gu , Xiaonan Hou , Elspeth Keating , Jianqiao Ye , Non-linear finite element model for dynamic analysis of high-speed valve train and coil collisions, *International Journal of Mechanical Sciences* (2020), doi: https://doi.org/10.1016/j.ijmecsci.2020.105476

Highlights:

- An engine head test is conducted on the valve spring to validate simulation results.

- A dynamical analytical model is used to simulate dynamical valve spring responses

- A transient finite element model is developed to simulate spring operations at high engine speeds

- The spring surge is simulated in a variable pitch spring at various engine speeds

- The phenomenon of usual significant spring forces caused by coil clash is simulated

# Non-linear finite element model for dynamic analysis of high-speed valve train and coil collisions

Zewen Gu[a], Xiaonan Hou[a, *], Elspeth Keating[b], Jianqiao Ye[a]

[a] Department of Engineering, Lancaster University, Lancaster LA1 4YW, UK
[b] WMG, University of Warwick CV4 7AL

## Abstract

A transient non-linear finite element (FE) model is developed in this paper to calculate the natural frequencies of a high-speed beehive spring and simulate its dynamic responses at different engine speeds, with consideration of material damping, internal vibration and coil collision. A 3D scanning technique is used to obtain an accurate geometry of the spring model for the simulation. To validate the FE model, a conventional analytical model with varying stiffness is also developed for the same spring. By comparing the results of both models with the experimental results of engine head tests, it is shown that the FE model can successfully simulate the dynamic responses of the spring under different speeds. Especially, the FE model can predict the erratic force spikes of the spring at high testing speeds, which cannot be predicted by the conventional analytical model. Based on the analysis, the dynamic deformation mechanisms of the high-speed beehive spring are summarised and discussed.

**Keywords**: Dynamics; Mechanics of material; Finite Element Simulation

## 1. Introduction

As the most flexible component in a valve train, the valve spring possesses the lowest elastic natural frequency. Other components that have much higher natural frequencies are usually treated as rigid bodies in a dynamic analysis [1, 2]. Valve springs, therefore, play a critical role in the dynamic analysis of a whole valve train [3-8]. Traditionally, valve springs were replaced by linear springs for simplification, and most of the studies primarily focused on the free vibration of helical springs, instead of studying the effects of the forced high-speed dynamics, using transfer matrix method [9], pseudo-spectral method [10] and Green's matrix method [11]. Consequently, the mechanisms of spring surge and coil clash were not emphasised. However, the surge of a valve spring, which can result in high spring stresses, is an essential factor in valve spring dynamics. It may cause higher maximum spring forces than those predicted from a linear static spring model. In practice, neglecting spring surge could lead to serious consequences, for instance, premature failure and malfunction of valve springs in valve trains. These failures occur more frequently at higher engine speeds. In order to simulate the effects of spring surges, several methods, such as distributed parameter model, multi-mass model and finite element model, have been developed. These models are reviewed below in details.

The distributed parameter model was used to simulate dynamic response of springs by Wahl in 1944 [12] and the method was then improved by Pisano et al [13]. In order to analyse the internal motion of a spring, a Modal analytical spring model was developed by solving the motion equation [13]. To simplify the calculation process, it was then used as a distributed parameter model where the dynamic response of a spring was treated as a superposition of harmonics modes [14]. The same Modal model was later implemented with a moving boundary technique to include the effects of coil clash at the lower spring end [15]. However, the location of the boundary should be traced accurately at each time step to achieve accurate dynamic forces. The computing time is therefore increased significantly. Beside the researches on the conventional valve springs, the Modal model was improved to study progressive valve springs [16, 17], by which the improved model was able to simulate the valve spring with varying natural frequencies. However, the effects of coil collisions were still excluded. For a better understanding of the relationships between valve springs and their connecting parts, a Modal spring model coupled with a finger-follower model was generated [18]. It was demonstrated that the modal model failed to simulate the force spikes caused by coil collisions, though the spike forces on the valve lifter were well simulated. More recently, the Modal model was improved by considering varying damping ratio during dynamic compression [19]. It proved that accurate dynamic results could be obtained by defining the damping ratio empirically.

Another popular method for analysing valve springs is the discrete mass model, or multi-body model. Discrete models that consist of two masses [20, 21], five masses [22], nine masses [23] have been developed.

These masses were connected by dampers and springs. Damping ratios of the dampers and stiffness of the springs were obtained from linear functions or static experiments. The method was also used by Prabakar et al [24] to simulate a dual-spring valve train system. To analyse the contacts between coils, the lowest mass of the total seven masses with a closer pitch was added into the normal multi-body model [25]. It was able to detect the coil contacts occurring on this mass. However, there are some limitations for the discrete mass model. Firstly, the stiffness of the springs connecting masses were used to calculate the vibration and impact forces. Therefore, these must be well defined to achieve accurate dynamic results. Secondly, regarding model properties, the multi-mass models only consider the coil contacts between the last two masses and coil clash between other coils are neglected. In addition, most of the multi-body spring models are one-dimensional, neglecting the effects of transverse vibration. The coupled discrete mass model was also applied to study nonlinear vibration of coupled oscillator systems. A system with two masses connected with linear and nonlinear springs was studied [26] by applying the called energy balance method (EBM). In later papers [27, 28] a mass-spring system with two masses and two springs was analysed using Hamiltonian Approach (HA) to achieve the accurate solution for the vibration of two-degree-of-freedom system. Results in these papers are in close agreement with the exact numerical value even with the presence of the nonlinear springs in the vibration systems.

The finite element (FE) model was applied in the analysis of valve spring dynamics by Kim et al [29] to study the dynamic response of a spring at 8200-rpm engine speed. However, the valve spring was assumed to have constant stiffness, uniform spring diameter and no coil clash, though the overall valve train system was nonlinear. A FE spring model using rod elements was applied in Lee's study [30], which considered the dynamic response of a spring in a two dimensional space. The FE model was later used to study the response of free vibrations of barrel, hyperbolical and conical springs [31]. A new method was developed by Huber and Clauberg [1, 2, 32] to simulate the dynamic response of valve springs at 2000-rpm, 4000-rpm and 6000-rpm engine speeds, respectively. In these studies, the valve springs were assumed as curved beams, from which hyperbolic partial differential equations were derived. These equations were discretised by FE method to calculate the dynamic forces of the valve springs. The simulation results agreed well with the measured spring forces at different engine speeds. However, spike forces observed at 6000-rpm engine speed were not explained by the model.

To the authors' best knowledge, there have been significant efforts made on the dynamic responses of high speed springs. However, most of the research focused on springs at an engine speed lower than 5000-rpm [1, 2, 13, 15-17, 19, 20, 23]. Though there are a few studies analyzing springs at higher engine speeds (> 5000-rpm) [14, 25, 29, 33], the abnormal high-frequency spike forces were usually ignored. In addition, there is a trend showing that unique pitch curves are introduced in new designs of springs to develop nonlinear springs with changeable natural frequencies. By introducing narrow pitches in these designs, contacts between spring coils are allowed. Consequently, the natural frequencies of the springs alter during spring surging. Many valve springs have varying spring diameters, which help to damp the internal vibrations. However, there are insufficient works that include this effect.

The objective of this study is to develop a transient finite element (FE) model to analyse the dynamic response of a high speed beehive valve spring, which has a varying spring diameter and narrow pitches. Using the developed model, the effects of coil collision, uneven spring diameter, varying spring stiffness, and therefore varying natural frequency on the overall dynamic response of the spring are discussed by comparing with a conventional analytical model and experiments. Especially, the unusual dynamic response of the valve spring at high engine speeds can be well simulated. The causes of spike spring forces at high engine speeds will be explained in detail by the transient FE model.

## 2. Analytical Modal Model Considering Varied Stiffness

An analytical model based on distributed parameter method is developed to compare its results with those of the FE model. In order to investigate the dynamic response of a spring, one can assume that spring show wave propagation of disturbances. The distributed parameter method can be applied to simulate the springs. In the method, the spring is discretized to small spring elements that are governed by the wave equation. In this paper, the investigated valve spring is considered running under different engine speeds, and both ends are fixed. The following derived differential equation Eq.(1) describes the motion of a spring element $\psi$ at position x and time t [12]. It is in the same form as the widely known equation for longitudinal wave transmission.

$$\frac{\partial^2 \psi}{\partial t^2} = c^2 \frac{\partial^2 \psi}{\partial x^2} \tag{1}$$

In this, the wave speed $c$ is a constant, i.e. $c = \sqrt{L^2 k / m}$ : $L$ is spring length; $k$ is spring stiffness; x denotes element position; $t$ is time and m is the active spring mass. The internal vibration of the spring is considered as a superposition of eigenmodes [14, 16]. In order to simulate the dynamic response of each modes, Eq. (1) is transferred to the form of a damped harmonic oscillator as shown by Eq. (2). The second term with damping ratio $\zeta$ in Eq. (2) is added to include the effects of damping.

The dynamic response of mode $n$ can be achieved by solving $G_n$. Details and solutions of Eq. (1) and Eq. (2) can be found as published by Phlips, Schamel and Meyer [14], Schamel, Hammacher and Utsch [16], Schamel [17] and Liu and Kim [19]. The spring dynamic response problem is eventually reduced to a set of ordinary differential equations.

$$\frac{d^2 G_n}{d\theta^2} + 2\zeta \frac{\omega_n(\theta)}{\omega_{cs}} \frac{dG_n}{d\theta} + \frac{\omega_n(\theta)^2}{\omega_{cs}^2} G_n = -\frac{2}{n\pi} \frac{d^2 y}{d\theta^2} \tag{2}$$

where, $\omega_{cs}$ is the cam speed, $\theta$ is the rotating cam angle, $y$ is the excitation curve, $G_n$ is the dynamic response of spring in mode $n$ and $\omega_n$ is the $n^{\text{th}}$ order natural frequency of the valve spring. Both y and $G_n$ are functions of cam angle θ. It is known that, in a normal car engine, the engine speed can always achieved by doubling the value of cam speed $\omega_{cs}$. The frequencies of the first three orders were calculated by a FE Modal analysis (Table 1) and used in this analytical model. The equation can be solved by transferring $G_n$ and $y$ into Fourier series (Eq. 3 and 4) as they are periodic and repeat over each cam cycle.

$$G_n(\theta) = \sum_{j=0}^{\infty} \left( a_j cosj\theta + b_j sinj\theta \right) \tag{3}$$

$$y(\theta) = \sum_{j=0}^{\infty} \left( e_j cosj\theta + f_j sinj\theta \right) \tag{4}$$

where $a_j$, $b_j$ and $e_j$, $f_j$ are the Fourier coefficients for the Fourier series of $Gn$ and $y$ respectively. The summation of the elastic modes $G_n$ can be solved by substituting Eq. (3) and (4) into Eq. (2). In order to calculate the total force of the valve spring, Eq. (5) used in the previous studies [12, 14, 16, 19] is adopted.

$$F_t = k(x) \cdot x_0 + k(x) \cdot y(\theta) + \pi k(x) \sum_n n G_n(\theta) \tag{5}$$

where $F_t$ is the overall spring force during operation, $x_0$ is the spring compression with a fitted height, $k$ is the stiffness of the spring, which is usually treated as a constant in the existing studies [14, 16, 17, 19]. However, it is not suitable to represent the spring with varying spring diameter and narrow pitches to be discussed in this paper. Hence, the constant stiffness $k$ is replaced by a variable $k(x)$. The formula of $k(x)$ with respect to spring compression is derived from the result of a static compression simulation (Figure 3). Thus, the first term, $k(x) \cdot x_0$, gives the initial spring force at the fitted height. The second term and the last term show the static and dynamic responses separately, where the varying stiffness $k(x)$ has been considered. The natural frequency $\omega_n$ used in Eq.(2) has a constant value of 630 Hz at the fitted height, the value of which is obtained from the FE Analysis model (Figure 4). Eventually, the non-linearity of varying spring stiffness during cam operation is included by replace term $k$ by $k(x)$. The nonlinear effects of coil clash are not considered in the analytical model.

## 3. Finite Element Model

### 3.1. Geometry and material properties

To develop a finite element model for high speed beehive valve springs, a geometry model was created using Solidworks. Instead of using design specifications, 3D scanning data of a spring was used to construct the model presented in Figure 1a. As shown in Figure 1(b-d), the 3D scanning profile of the manufactured spring is different to the original design specifications.

For the coil diameter, there is a misalignment between the one based on the scanning data and the one based on the design specifications after coil number 4, as shown in Figure 1b. The diameter based on the design specifications decreases linearly from coil 4 to the top end (coil 7), while, the diameter based on the scanning data decreases in steps. Based on the design specifications, the height should increase linearly from coil 1 (the bottom) to coil 7 (the top), as seen in (Fig. 1c). However, the height based on the scanning data increases with several fluctuations, which reflects the features of the real product. The real pitch based on the scanning data shows different values to the one based on the design specifications. According to the design specifications, the pitch should vary linearly from coils 1 to 3, keep at a constant level from coils 3 to 6 and then decrease linearly from coils 6 to 7 (Figure 1d). Based on the scanning date, the change of the pitch against the coil number shows deviations from the one defined by the design specifications, which may be due to the manufacturing tolerance and the deformations due to the residual stresses produced during the manufacturing process. The deviations in geometric features may significantly affect the natural frequency, stiffness and self-contact, in other words the performance of the spring [12, 34]. Therefore, the scanning data was used in the FE analysis in this study to include these effects.

The material used to fabricate the spring is super clean (SC) spring steel OTEVA 90. The density is 7850 kg/m$^3$, Young's Modulus is 206 GPa and shear modulus is 79.6 GPa. The material used for the retainer and the spring seat is structural steel, density 7850 kg/m$^3$, Young's Modulus 200 GPa and shear modulus 76.9 GPa. The 3D beehive spring geomerty was constructed from the scanning data. It was then exported to build the FE model in Ansys Workbench as shown in Figure 2.

### 3.2. Static and Modal FE Analyses

The spring surge is mainly caused by internal vibrations of a valve spring. Hence, the natural frequency of the spring is directly associated with the shapes, magnitudes and frequency of the internal vibration. The beehive valve spring is fitted into an engine with a 7 mm pre-compression. To simulate the effect of the pre-compression, a static FE model was developed (Figure 2a) using the commercial software Ansys Workbench. There are two different types of elements in the model, the hexahedron element and the tetrahedron element. A hexahedron element is a topological cube that has 8 vertices, 12 edges, bounded by 6 quadrilateral faces. It provides high accuracy of solutions for the same element amounts. In this paper, it is used to mesh the spring coils 02, 03, 04, 05 and 06. A tetrahedron element has 4 vertices, 6 edges, and is bounded by 4 triangular faces. Considering that the spring coils 01 and 07 are grounded that have complex geometries, the tetrahedron element is used to mesh the spring coils 01 and 07. In addition, a retainer was developed on the top of the spring model, and a valve seat was developed underneath the spring. Both of them were meshed by hexahedron elements. In total, 160245 elements were used for the static FE model. To fix the spring in between the retainer and the valve seat, the upper (Figure 2b) and the lower end faces (Figure 2c) of the spring were bonded with the retainer and spring seat, respectively (Figure 2a). Frictionless contact is defined across the elements of the whole spring geometry to consider the effects of internal contact during vibration. To apply the load, the bottom of the spring seat was fixed in all six degrees of freedom. A 7 mm displacement was applied on the retainer (Figure 2a) along the z axis. All others degrees of freedom were fixed. The deformed FE spring model under the 7 mm pre-compression is shown in Figure 2d. It is noted that coil 2 is compressed onto coil 1. The spring force of the static compression test and the static FE simulation are shown Figure 3. The slopes of the two curves, which also represent the stiffness of the spring, change slightly at around 5 mm compression. It illustrates that the stiffness is changing as coils collapse during operations. The deformed spring, together with the static stresses recorded in the elements was imported to a modal FE model. In the modal model, both the end faces of the spring (Figure 2(b-c)) were fixed. Figure 4(a-c) display the displacement of the first three modes of vibration in the longitudinal direction. The FE Modal analysis shows the vibration modes as those predicted by the classic theory shown in Figure 4d. In the first mode, the phase motion of the entire valve spring is to the same spring end. The centre part of the spring has the largest

amplitude. In the second mode (Figure 4b), the upper part and lower part of the spring move in antiphase. In the third mode, the phase motion has a similar behaviour as that in the second mode (Figure 4c). The simulated frequencies of the first three modes are shown in Table 1.They have been used in the analytical modal analysis in Eq. (2).

### 3.3. Transient analysis settings and boundary conditions

To simulate the dynamic response of the 3D beehive spring, a transient FE model (Figure 5a) was developed based on the geometric model with the pre-load obtained by the static FE model (Figure 2d). In this model, the regions at both the upper (coil 07) and the lower (coil 01) ends of the spring were meshed using refined elements. It can be seen that coil 01 and coil 07 have finer meshes than that of the middle portion as coil collisions are expected to occur repeatedly at these regions at a high loading speed. In total, 160245 elements were used in this model. The size function of curvature and mixed element types of tetrahedron and hexahedron were used for meshing. The material properties are unchanged. The damping ratio was defined as 0.016, which is an empirical value used by most of relevant studies [19, 35]. The lowest harmonics frequency of the spring was 630 Hz (Table 1). The damping ratio and the frequency were used to determine the Rayleigh Damping coefficients for this transient model. To simulate the constraints of the spring, the end faces of coil 01 and coil 07 were bonded with the retainer and the valve seat, respectively. The bottom of the spring seat was fixed and the loading was applied on the top surface of the retainer. As shown in Figure 5a, Node 01 is located at the centre of the cross-section of the end of coil 01. Similarly, Node 02 is the central node of the cross-section of the end of coil 02. These nodes are used in the analysis of the internal vibrations of the spring, as well as to determine coil collision occurrence.

The cam stroke curve (Figure 6) is the applied dynamic loading for one cam cycle. It can be divided into three operation stages, i.e., Stage I (0-127 degree of cam angle), Stage II (127-233 degree) and Stage III (233-360 degree). At stage I, the spring carries zero (0-90 degree) or very low (90-127 degree) external loading that increases with the cam angle. It means that the spring almost moves under free vibration. At the Stage II, a large valve lift displacement is applied, when the cam angle increases from 127 to 233 degree. At the final stage (Stage III), the external loading becomes very low due to the profile of the cam. When the cam angle reaches 270 degree, the loading becomes zero, similar to the loading condition at Stage I.

The spring FE model was firstly compressed by the 7 mm install height to simulate the fixture of the valve spring (Figure 2d). As a result, the transient simulation started with a 289 N pre-load at the install height. 72 steps were taken in the analysis of one cam cycle. For each step, there were 10 sub-steps, which gave a total of 720 time steps for an entire cam cycle. Three different engine speeds, namely 4200-rpm, 5600-rpm and 8000-rpm were used in the simulations. The corresponding cam speeds and the time steps are listed in Table 2. For each testing speed, two continuous cam cycles were simulated as shown in Figure 7. However, only the results of the second cam cycle (Cycle II) of every engine speed were analysed as the first cycle starts from a stationary state, as shown in Figure 7, which is not a representative cam cycle of a working spring. The second cam cycle (Cycle II) started with the residual spring vibration from Cycle I, which could represent realistic loading conditions of the spring. The reaction force of the lower end of the spring (Figure 2c) was recorded at each time step of cycle II. The displacement, velocity and acceleration of Node 01 and Node 02 (Figure 5a) were extracted to analyse the internal vibration and coil collision.

## 4. Results and discussions

### 4.1. Dynamic response at 4200-rpm engine speed

To analyse the dynamic response of the spring, the results obtained from both the FE and the analytical models are compared with the results of engine head tests. When the loading speed is 4200-rpm, the spring force with respect to the cam angle is shown in Figure 8. It is clear that the spring force oscillates over a range of 12 N (from 270 N to 282 N) at stage I, which is a free vibration due to the residual energy from the previous cam cycle. With the rotation of the cam, the spring starts to be compressed by a large valve lift (Stage II), when the cam angle is 127 degree. The reaction force increases significantly until the cam angle is around 183 degree, where peak forces are obtained. The magnitudes are 818 N, 814 N and 806 N for the FE model, analytical model and experiment, respectively. Then, the reaction force decreases until the cam angle reaches 233 degree (the end of Stage II). In general, both the FE and the analytical models can describe the dynamic response of the spring with good agreements to the test results. However, according to the test results,

there are high-frequency vibrations when the cam angle is around 235 degree, which is due to the internal contacts of spring coils. As can be seen in Figure 8, the FE model can simulate the phenomena, while the analytical model does not provide adequate detail of the occurrence.

To analyse the internal motion of the spring coils, the two reference nodes, Node 01 and Node 02 are marked as shown in Figure 5a. The accelerations, velocities and displacements of the nodes along the Z axis at 4200-rpm are given in Figure 9. It is noteworthy that the displacement of Node 02 is obtained by recording the co-ordinate positions of Node 02, where the distance between coil 01 and coil 02 at all cam angles has been subtracted. Therefore, a zero value of it indicates that coil 02 is touching coil 01. Within the cycle, the displacement of Node 01 (Figure 9a) is almost constant and close to zero, which means that coil 01 experiences no significant longitudinal motion. Node 02 (Figure 9a) oscillates freely at the beginning of stage I, which is due to the residual vibrations from Cycle I. At the end of stage I, the effect of free vibration reduces due to the effects of damping and the compression of the external loading. At the beginning of Stage II, the compressive displacement is 0.07 mm, when coil 02 makes contact to coil 01. Both coils 01 and 02 deform elastically, which explains that the negative values in this stage. During Stage III, Node 02 starts to vibrate freely under a certain frequency.

As shown in Figure 9b, the velocity of Node 01 keeps constant in the entire cam cycle which shows that coil 01 does not move. For Node 02, its velocity varies slightly during Stage I and Stage II. It indicates that coil 02 moves due to the residual vibration at stage I and oscillates with a higher frequency due to the contact with coil 01. At Stage III, the velocity of Node 02 changes rapidly. The points of these rapid changes are also the ones where the displacement of Node 02 changes significantly (Fig. 8a). The acceleration responses of Node 01 and Node 02 are presented in Figure 9c. The acceleration of Node 01 keeps at a very low level during Stages I and II, although there are fluctuations around 140 degree and 160 degree. During Stage III, the acceleration varies at a higher level. The fluctuations are around 280 degree, 300 degree and 315 degree. The peak acceleration of Node 01 is approximate $-4.24e6$ mm/s$^2$ occurred at 315.5 degree of cam angle at Stage III. For Node 2, the trend is similar to Node 1. However, the magnitudes of the fluctuations are higher than those of Node 01. The peak acceleration, approximate $5.49e6$ mm/s$^2$, of Node 02 occurs at around 314 degree at Stage III. The peak accelerations of both Node 02 and Node 01 are consequences of the rapid changes of velocities, which is due to the coil collisions between coil 01 and coil 02.

According to the results of the FE simulation, it can be concluded that coil 02 vibrates freely at Stage I and Stage III. During Stage II, it is compressed to contact coil 01 by external loading, and there is no separation between the two coils. During Stage III, the rapid changes on velocity and acceleration of Node 02 are also caused by the contact between coils 1 and 2, which could explain the high-frequency fluctuations of the spring force around 165 degree, 235 degree, 280 degree, 300 degree and 315 degree of cam angle.

## 4.2. Dynamic response at 5600-rpm engine speed

The results of dynamic response of the valve spring at 5600-rpm engine speed are displayed in Figure 10. At Stage I, the spring force starts to oscillate within a range between 250 N and 350 N, which is approximate 90 N larger than the one at 4200-rpm engine speed. Then, the spring is compressed significantly at the beginning of Stage II (127 degree of cam angle). The spring force increases until the cam angle is around 175 degree, where the peak force is obtained. The magnitudes obtained from the FE model, the analytical model and the experiment are 896 N, 865 N and 845 N, respectively. It is clear that the peak forces in Stage II at 5600-rpm are about 60 N higher in average than those at 4200-rpm. It means that the dynamic effects of both the natural vibration and the forced motion are greater due to the increase of engine speed. After 175 degree of cam angle, the spring force decreases until the cam angle is 233 degree (the end of Stage II). The loading starts to be removed at the beginning of Stage III, and the spring vibrates freely. Both analytical model and FE model well fit the experimental curve at the Stage I and Stage II. However, high-frequency spring forces are detected in both the FE model and the experiment results around 240 degree of cam angle, when the analytical model fails to show this effect. The maximum values of these spike forces is as high as 620 N, which is about 305 N higher than that at 4200-rpm. The peak force obtained from the analytical model is 380 N at this point of time.

The accelerations, velocities and displacements of the reference nodes along the Z axis at 5600-rpm are given in Figure 11. Similar to the results at 4200-rpm, the displacement of Node 01 keeps constant during the whole cam cycle in Figure 11a, because the end of this coil is fixed. The displacement of Node 02 oscillates regularly during Stage I. It illustrates that coil 2 vibrates freely starting with the residual vibration of previous cam cycle. The magnitude of the displacement can reach as high as around 0.2 mm, which is nearly 10 times the one at 4200-rpm. During Stage II, the displacement keeps nearly a constant. It is because coil 02 is pressed

onto coil 01 by the external loading. At the beginning of Stage III, it starts to fluctuate at a high frequency. As shown in Figure 11b, the velocity of Node 01 is around zero during the whole cam cycle, which is corresponding to its constant displacement shown in Figure 11a. On the other hand, the velocity of Node 02 fluctuates with a range of 1290 N (from -742 mm/s to 548 mm/s) in Stage I. It is reduced, then, to zero during Stage II due to the external compressive loading. During Stage III, it reaches to a peak velocity of 1352 N/mm at 241.5 degree toward the negative direction of the z axis after a 1000 mm/s velocity toward the z axis. Then, it fluctuates with a range of 1598 mm/s (from -978 mm/s to 620 mm/s). The accelerations of Node 01 and Node 02 are displayed in Figure 11c. The acceleration of Node 01 is nearly constant during Stage II while spike accelerations appear at 20 degree, 46.5 degree, 73 degree, 100 degree, around 245.5 degree, 300 degree, 328 degree and 354.5 degree, respectively, during Stage I and Stage III. Another phenomenon is that the spike accelerations of Node 02 always appear at the same time. It means that coil collisions occur between coil 01 and 02 at those times. Contact status between coil 01 and coil 02 at three different cam angles is shown in Figure 12. The areas where coil 02 contacts coil 01 are in pink. 'Sliding' indicates that there are transverse slides between contact surfaces. The areas in yellow named as 'near' indicating that coil 01 and coil 02 are close but still separated. From cam angle 240 degree to 245.5 degree, the two coils experience a contact-separation-contact process within a 0.327e-3 second. The process indicates a violent coil collision, and explains the spike forces occurring at the time points.

Comparing to the dynamic response at 4200-rpm, the spring force is generally higher due to the higher loading speed of 5600-rpm. The high-frequency fluctuations also appear at the beginning of Stage III. However, the spike forces are much higher than the ones at 4200-rpm, caused by the violent coil collisions.

### 4.3. Dynamic response at 8000-rpm engine speed

Figure 13 shows the dynamic responses of the valve spring at 8000-rpm engine speed. The zoomed in area shown in Figure 14 displays a greater details of Stage III, during which the peak forces occurred. At Stage I, the spring force oscillates at a range of 200 N (between 250 N and 450 N), which is approximate 100 N larger than the magnitude (100 N) at 5600-rpm and 190N larger than the one (10 N) at 4200-rpm engine speed. The frequencies of the vibration obtained from the FE model generally agree with the ones from experiments. However, a phase difference is observed in the result of the analytical model. For instance, the first three peak forces appear at 12.5 degree, 42 degree and 84.5 degree from the FE model and test results, while they appear at 24 degree, 58 degree and 100 degree in the analytical model. The phase difference is approximately 15 degree. When the spring is compressed at Stage II, the spring force increases to the first peak, around 940 N in the FE model (895 N from test), at about 160 degree of cam angle. However, the force curve of the analytical model reaches its peak force (880 N) at 170 degree of cam angle, thus, represents a phase lag of 10 degree. With the rotation of the cam, the force decreases to around 580N in the FE model (581 N from test) at approximate 172 degree. When the cam angle is 186.5 degree, the force increases again and reaches its second peak value, around 1200 N in the FE model (1051 N from test). The second peak of the force based on the analytical model is 778 N at 203 degree, where the lag is 16.5 degree comparing with the results of the FE model and the experiment. After the second peak, the force keeps decreasing until 250 N at the end of Stage II (233 degree). At Stage III, the change of the force is mainly dominated by a free vibration due to the low external loading. During this stage, very high spike forces are obtained. For instance, the spring force reaches as high as 1430 N at 254.5 degree from both the FE model and the test results, which is even higher than the peak force in Stage II. However, the peak force calculated by the analytical model is only 360N, when the cam angle is270 degree. The results show that the analytical model is not capable of simulating dynamic responses of the valve spring at a relative high engine speed.

To understand the internal vibrations of the spring at 8000-rpm engine speed, the accelerations, velocities and displacements of Node 01 and Node 02 are shown in Figure 15. At Stage I, the displacement of Node 01 (Figure 15a) remains constant and is close to 0 mm. The displacement of Node 02 (Figure 15a) oscillates in a range of 0.17 mm. By comparing to the results at 4200-rpm and at 5600-rpm, it appears more irregularly. At Stage II, there is nearly no movement when the external loading is executed. It illustrates that coil 02 is nearly compacted onto coil 01 despite very small vibrations at 155 degree and 185 degree. At the end of Stage II (233 degree), Node 02 begins to move upward. It reaches its maximum displacement 0.68 mm, when the cam angle is around 243 degree (Stage III). It is about 0.4 mm and 0.63 mm higher than the magnitudes at 5600-rpm and 4200-rpm respectively. Then, the force starts to oscillate irregularly. The velocities of Nodes 01 and 02 are displayed in Figure 15b. The velocity of Node 01 remains nearly constant throughout the whole Stage I, II and III, though slight vibration observed at 270 degree and 300 degree in Stage III. For Node 02, the

magnitude of velocity varies irregularly within a range of 1320 mm/s at Stage I. Then it keeps nearly zero during Stage II except two fluctuations of velocities occurs at 155 degree and 185 degrees. At the beginning of Stage III, the magnitude increases significantly from 0 mm/s (232 degree) to 2130 mm/s (238.5 degree), and then dramatically decreases by 4815 mm/s to -2685 mm/s at 251.5 degree. With a further rotation of the cam (from 251.5 degree to 252.5 degree), the velocity increases rapidly again, which is from -2685 mm/s to 811 mm/s. This process occurs within 41.6e-6 second. The magnitude varies arbitrarily during the rest of Stage III. Figure 15c shows the acceleration curves for Nodes 01 and 02. The acceleration of Node 01 has no obvious fluctuation in Stage I and Stage II. At stage III, there are some fluctuations where the peak values are 3.92e7 mm/s$^2$, 1.53e7 mm/s$^2$ and 3.07e7 mm/s$^2$ at 254.5 degree and 297 degree, respectively. For Node 2, the levels of fluctuations in Stage I and Stage II are lower comparing with the one in Stage III. When the cam angle is 254.5 degree, the acceleration reaches its maximum 1.03e8 mm/s$^2$, which is corresponding to the peak spring force at the same time. In addition, significant spike forces (Figure 13) also occur at these positions (254.5 degree and 297 degree). It can be therefore assumed that violent coil collision occurs between coil 01 and coil 02 at these times. The dynamic spring force is hugely lifted by these impact forces, which are shown by the significant spike forces in the final results.

Contact status between coil 01 and coil 02 at 8000-rpm is shown in Figure 16. It is shown that a contact-separation-contact process occurs, when the cam angle increase from 253.5 degree to 255.5 degree. The process occurs within 0.0832e-3 second. The violent coil collision explains the spike spring force at 254.5 degree. At 8000-rpm engine speed, the effects of coil collision on the spike forces are enhanced. The peak force of the spring occurs during Stage III due to the coil collision rather than external loading. The results of modal analyses do not show the spike forces caused by coil collisions, and certain phase difference is observed in the whole cam cycle. In sum, it shows that the FE model has a robust ability to simulate the dynamic effects of valve springs at this speed with a good agreement with the test results. On the contrary, the analytical modal model fails to be comparable with the test results at this speed.

## 5. Conclusion

In this paper, a nonlinear FE model has been developed to simulate the dynamic responses of a beehive valve spring at various engine speeds. Large deformations, varied spring diameter, varied spring pitch and therefore varied natural frequency, coil collisions are all considered in this model. An analytical modal model was also developed and its results were compared with those of the FE model. A set of engine head test results were used to validate the computational results of both models. According to the analysis of the results, the following conclusions are made:

1. By comparing with engine test results, both the FE modal and the analytical models are able to simulate the reaction force of the spring at Stage II of the deformation, when the engine speed is relative low (4200-rpm). At this speed, the reaction force is a result of both the external loading and the internal vibrations of the coils. However, the FE model can also simulate the high-frequency vibrations at the beginning of Stage III, when the analytical model fails to.

2. At relative higher engine speeds (5600 rpm), the peak reaction force is still determined by the external loading and natural frequency. Both the analytical and FE models can calculate the peak reaction force at Stage II accurately. However, the effects of coil collision become more significant with the increased engine speed. The unusual spike forces are observed at the stage III of the deformation in both the FE model and the testing results. Again, the analytical model cannot analyse the effects due to its intrinsic limitations.

3. At 8000-rpm engine speed, the peak dynamic force occurs at the stage III of the deformation, which is due to the dominating effect of coil collisions. The high frequency contact force between the coils results in the extreme high spike reaction force, which is absent from the analytical model. In practices, the analytical model is still widely used in the design and analysis of valve springs. Therefore, the dynamic factor of the spring is likely to be underestimated by the analytical model, which may cause premature failure of the valve spring. For a more reliable spring design, the new FE model developed in this paper can be used to predict the reaction forces at different engine speeds, including extreme high speeds.

**Acknowledgements**

## CRediT author statement

**Zewen Gu:** Writing - Original Draft, Software, Formal analysis, Validation, Methodology
**Xiaonan Hou:** Conceptualization, Methodology, Writing- Reviewing and Editing, Funding acquisition
**Elspeth Keating:** Writing- Reviewing and Editing, Visualization
**Jianqiao Ye:** Supervision, Writing- Reviewing and Editing, Funding acquisition

## Reference

[1] R. Huber, J. Clauberg, H. Ulbrich, An efficient spring model based on a curved beam with non-smooth contact mechanics for valve train simulations, SAE International Journal of Engines, 3 (2010) 28-34.
[2] J. Clauberg, B. Huber, H. Ulbrich, Simulation and Validation of Valve Springs in Valve Train Simulations, in: Proceedings of the Eighth International Conference on Engineering Computational Technology, 2012.
[3] M. Koster, Effect of flexibility of driving shaft on the dynamic behavior of a cam mechanism, Journal of Engineering for Industry, 97 (1975) 595-602.
[4] K. Nagaya, K. Watanabe, Y. Tsukahara, Vibration analysis of high rigidity driven valve system of internal combustion engines, Journal of sound and vibration, 165 (1993) 31-43.
[5] Y.S. Ünlüsoy, S.T. Tümer, Analytical dynamic response of elastic cam-follower systems with distributed parameter return spring, Journal of Mechanical Design, 115 (1993) 612-620.
[6] Y. Ünlüsoy, S. Tümer, Non-linear dynamic model and its solution for a high speed cam mechanism with coulomb friction, Journal of sound and vibration, 169 (1994) 395-407.
[7] T. Dresner, P. Barkan, New methods for the dynamic analysis of flexible single-input and multi-input cam-follower systems, Journal of Mechanical Design, 117 (1995) 150-155.
[8] D.-J. Chun, J.-K. Lee, An analysis of valve train behavior considering stiffness effects, KSME international journal, 14 (2000) 283-290.
[9] V. Yildirim, N. İnce, Natural frequencies of helical springs of arbitrary shape, Journal of Sound and Vibration, 204 (1997) 311-329.
[10] J. Lee, Free vibration analysis of cylindrical helical springs by the pseudospectral method, Journal of Sound and Vibration, 302 (2007) 185-196.
[11] S.V. Sorokin, The Green's matrix and the boundary integral equations for analysis of time-harmonic dynamics of elastic helical springs, The Journal of the Acoustical Society of America, 129 (2011) 1315-1323.
[12] A.M. Wahl, Mechanical springs, Penton Publishing Company, 1944.
[13] A. Pisano, F. Freudenstein, An experimental and analytical investigation of the dynamic response of a high-speed cam-follower system. Part 2: a combined, lumped/distributed parameter dynamic model, Journal of Mechanisms, Transmissions, and Automation in Design, 105 (1983) 699-704.
[14] P. Phlips, A. Schamel, J. Meyer, An efficient model for valvetrain and spring dynamics, in, SAE Technical Paper, 1989.
[15] Y. Lin, A. Pisano, Three-dimensional dynamic simulation of helical compression springs, Journal of Mechanical Design, 112 (1990) 529-537.
[16] A.R. Schamel, J. Hammacher, D. Utsch, Modeling and measurement techniques for valve spring dynamics in high revving internal combustion engines, SAE Transactions, (1993) 820-836.
[17] A. Schamel, A frequency domain approach to the analysis and optimization of valve spring dynamics, in, © A. Schamel, 1993.
[18] W. Hsu, A. Pisano, Modeling of a finger-follower cam system with verification in contact forces, Journal of Mechanical Design, 118 (1996) 132-137.

[19] H. Liu, D. Kim, Estimation of valve spring surge amplitude using the variable natural frequency and the damping ratio, International Journal of Automotive Technology, 12 (2011) 631.

[20] M. Kushwaha, H. Rahnejat, Z. Jin, Valve-train dynamics: a simplified tribo-elasto-multi-body analysis, Proceedings of the Institution of Mechanical Engineers, Part K: Journal of Multi-body Dynamics, 214 (2000) 95-110.

[21] M. Teodorescu, M. Kushwaha, H. Rahnejat, S. Rothberg, Multi-physics analysis of valve train systems: from system level to microscale interactions, Proceedings of the Institution of Mechanical Engineers, Part K: Journal of Multi-body Dynamics, 221 (2007) 349-361.

[22] S. Mclaughlin, I. Haque, Development of a multi-body simulation model of a Winston Cup valvetrain to study valve bounce, Proceedings of the Institution of Mechanical Engineers, Part K: Journal of Multi-body Dynamics, 216 (2002) 237-248.

[23] S. Seidlitz, Valve train dynamics-a computer study, in, SAE technical paper, 1989.

[24] R. Prabakar, A. Nagar, N. Umashankar, Multi-Body Dynamic Simulation and Experimental Validation of Valve Spring Surge Speed, in, SAE Technical Paper, 2013.

[25] T. Kitada, M. Kuchita, Development of vibration calculation code for engine valve-train, Mitsubishi Motors Technical Review, Report, (2008) 74-82.

[26] M. Bayat, M. Shahidi, A. Barari, G. Domairry, Analytical evaluation of the nonlinear vibration of coupled oscillator systems, Zeitschrift fuer Naturforschung A, 66 (2011) 67-74.

[27] M. Bayat, I. Pakar, Nonlinear dynamics of two degree of freedom systems with linear and nonlinear stiffnesses, Earthquake Engineering and Engineering Vibration, 12 (2013) 411-420.

[28] M. Bayat, I. Pakar, L. Cveticanin, Nonlinear free vibration of systems with inertia and static type cubic nonlinearities: an analytical approach, Mechanism and Machine Theory, 77 (2014) 50-58.

[29] D. Kim, J.W. David, A combined model for high speed valve train dynamics (partly linear and partly nonlinear), in, SAE Technical Paper, 1990.

[30] K. Lee, Dynamic contact analysis for the valvetrain dynamics of an internal combustion engine by finite element techniques, Proceedings of the Institution of Mechanical Engineers, Part D: Journal of Automobile Engineering, 218 (2004) 353-358.

[31] K. Girgin, Free vibration analysis of non-cylindrical helices with, variable cross-section by using mixed FEM, Journal of Sound and Vibration, 297 (2006) 931-945.

[32] J. Clauberg, R. Huber, Using non-smooth mechanics and parallelization techniques for the efficient simulation of different types of valve springs, in, SAE Technical Paper, 2013.

[33] Y. Takashima, T. Mizuno, T. Goto, M. Wakita, K. Hasegawa, Parametric design with valve train dynamic analysis and digital data based manufacturing of the valve spring, in, SAE Technical Paper, 2005.

[34] A.E.H. Love, A treatise on the mathematical theory of elasticity, Cambridge university press, 1972.

[35] J. Lee, D. Patterson, Nonlinear valve train dynamics simulation with a distributed parameter model of valve springs, Journal of engineering for gas turbines and power, 119 (1997) 692-698.

**Declaration of interests**

☒ The authors declare that they have no known competing financial interests or personal relationships that could have appeared to influence the work reported in this paper.

☐The authors declare the following financial interests/personal relationships which may be considered as potential competing interests:
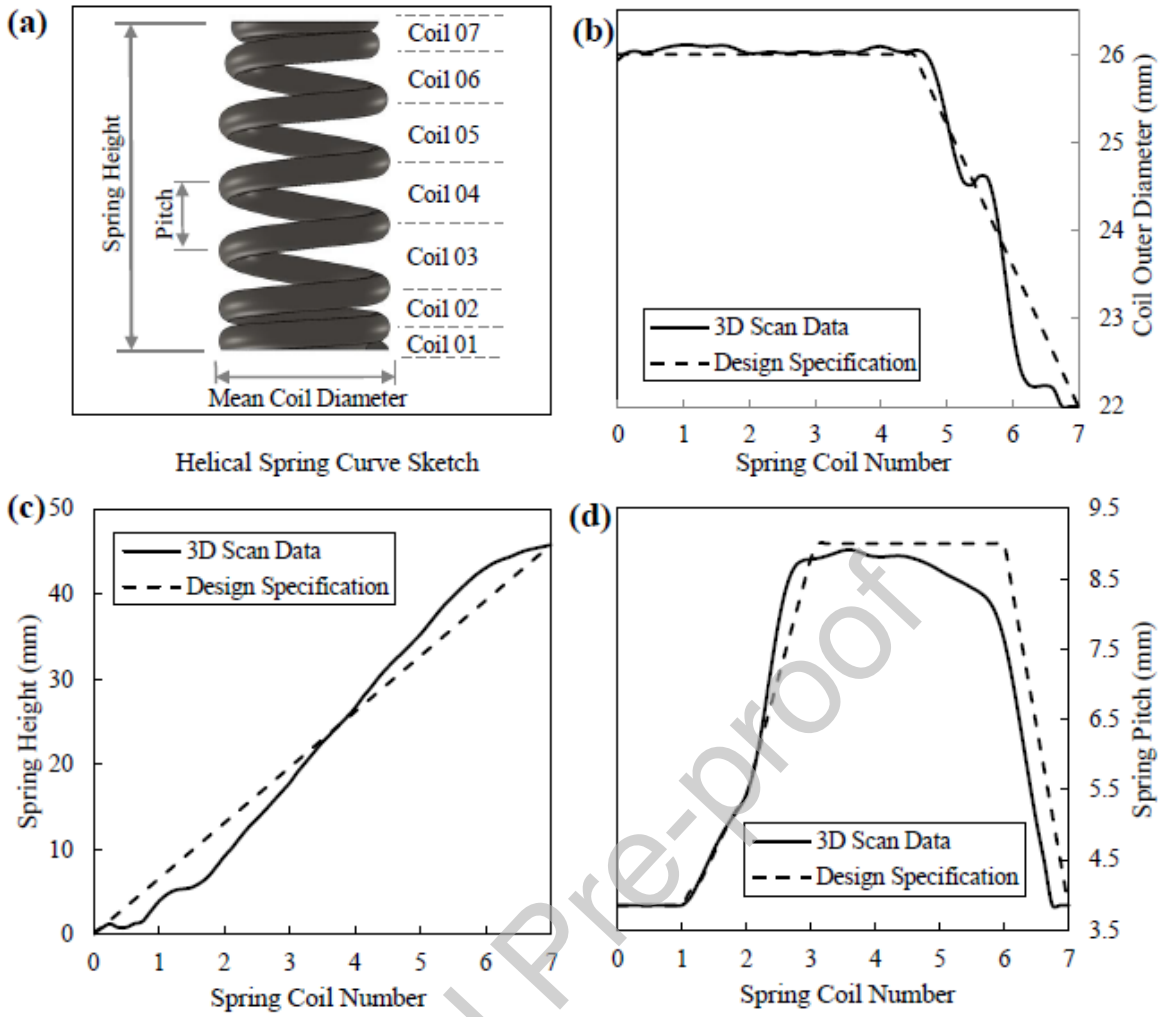
*Figure 1: (a). Spring Terminology. Design Specification and 3D Scan Data of (b). Spring Coil Outer Diameter, (c). Spring Height, and (d). Spring Pitch.*
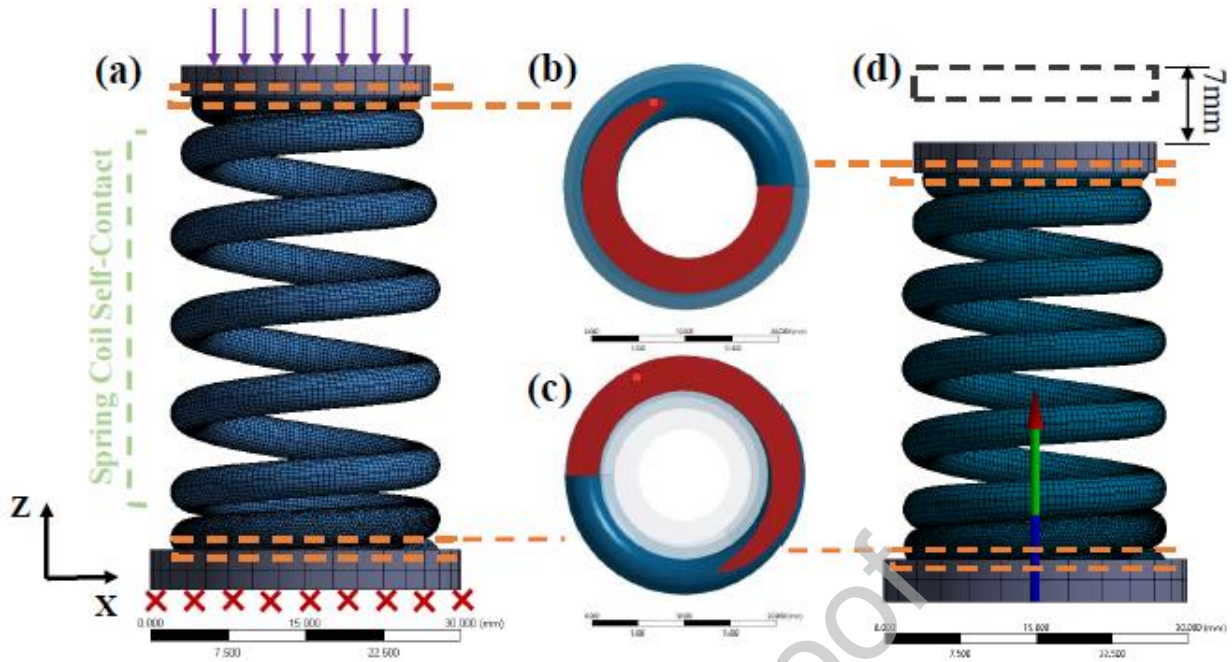
Figure 2: (a). Boundary conditions of Modal FE model, and the fixed (b). upper end and (c). lower end of the spring. (d). TheFEmodel with a 7mm pre-compression.
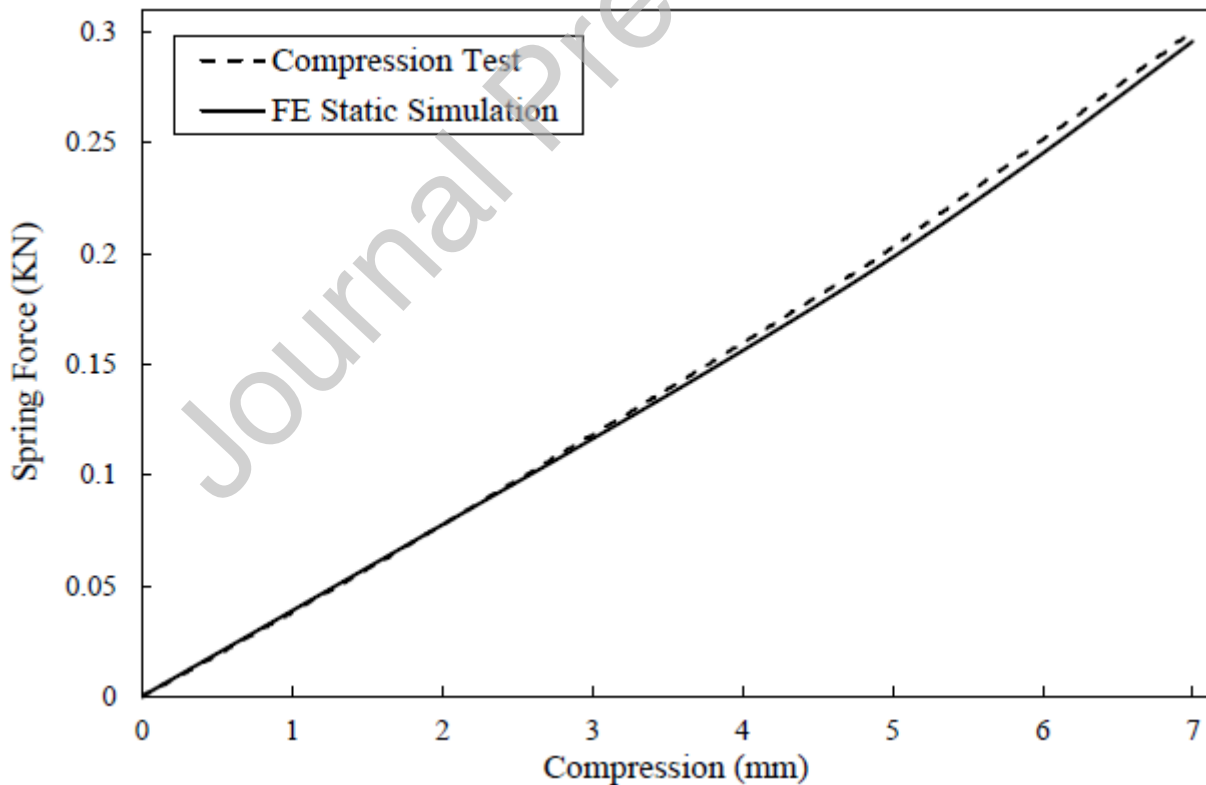


Figure 3: FE static 7 mm simulation validated by the results of compression test.
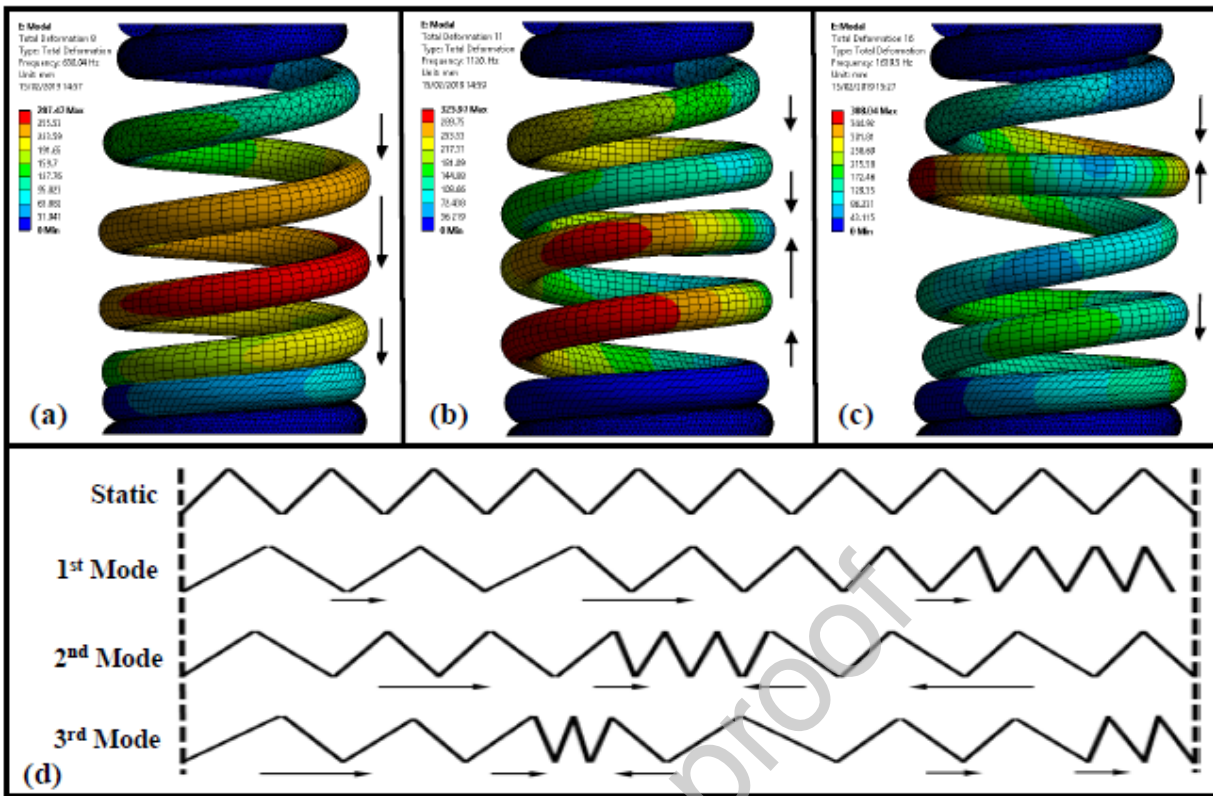
Figure 4: The simulated (a). First. (b). Second, and (c). Third modal modes in AnsysFE Modal Analysis. (d). the theoretical first three modal modes described in [16, 17, 32].
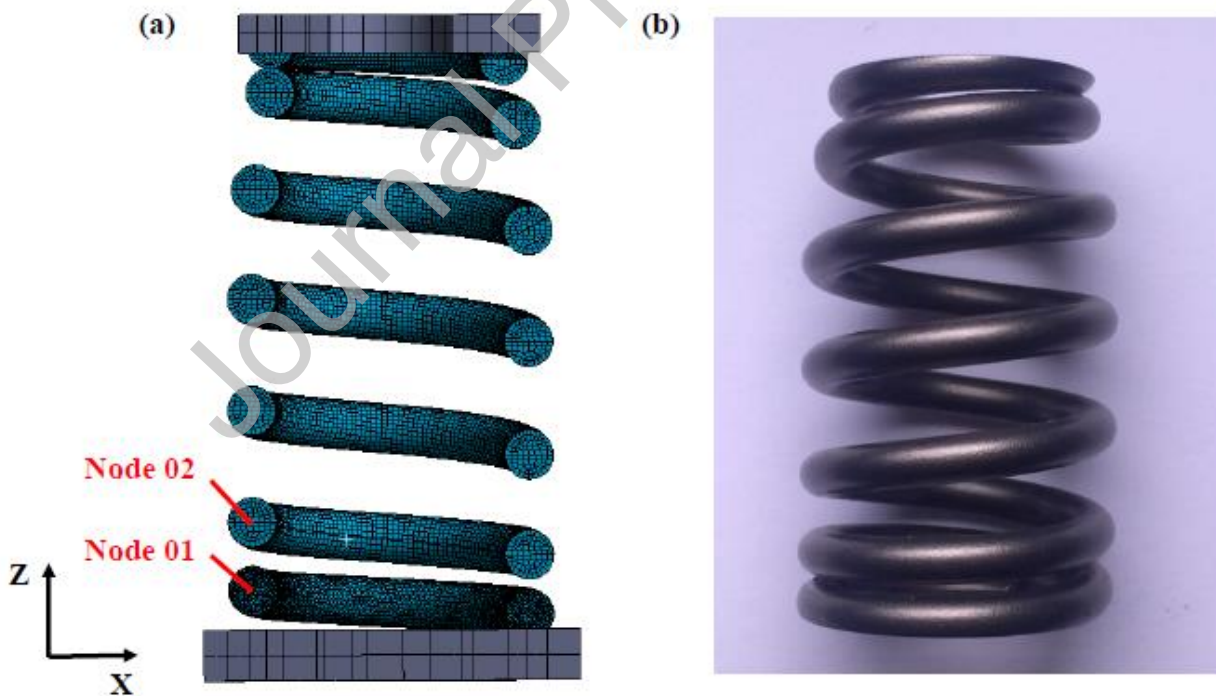


Figure 5: (a). Node Id selected in transient FE simulations. (b). Beehive spring sample manufactured by Force Technology Ltd.
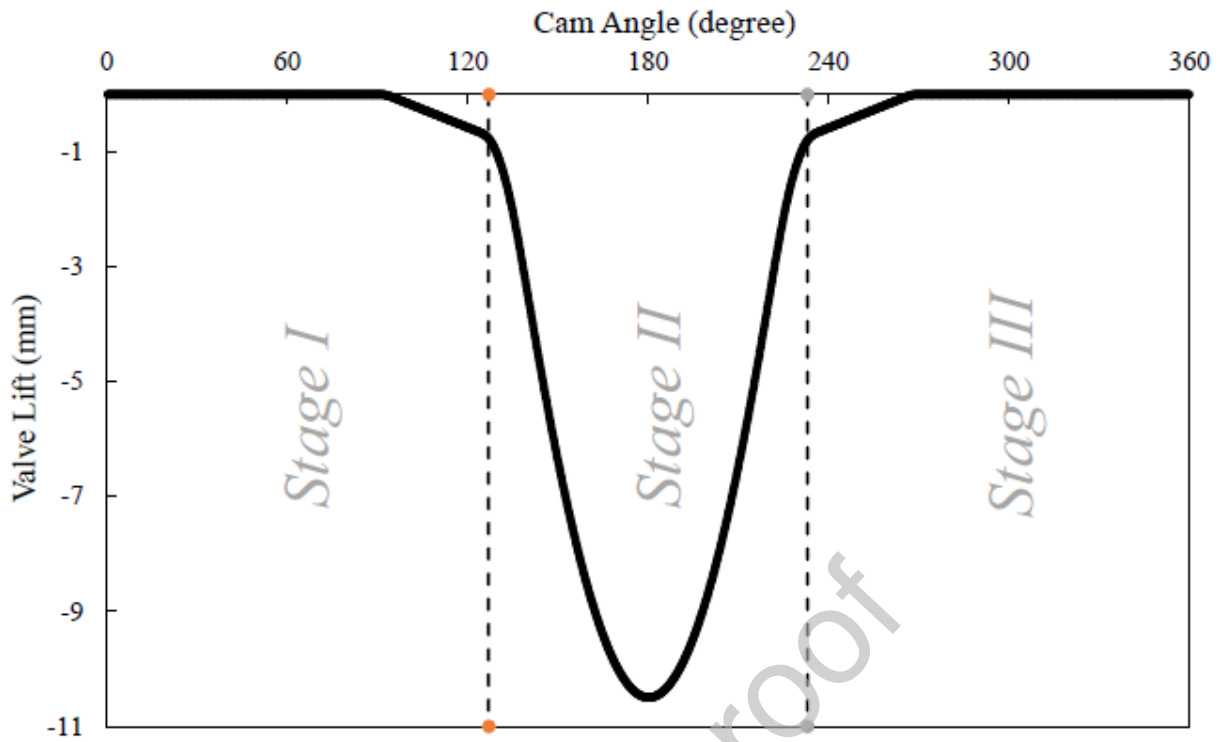
*Figure 6: Valve lift curve of the beehive valve spring in the real engine.*
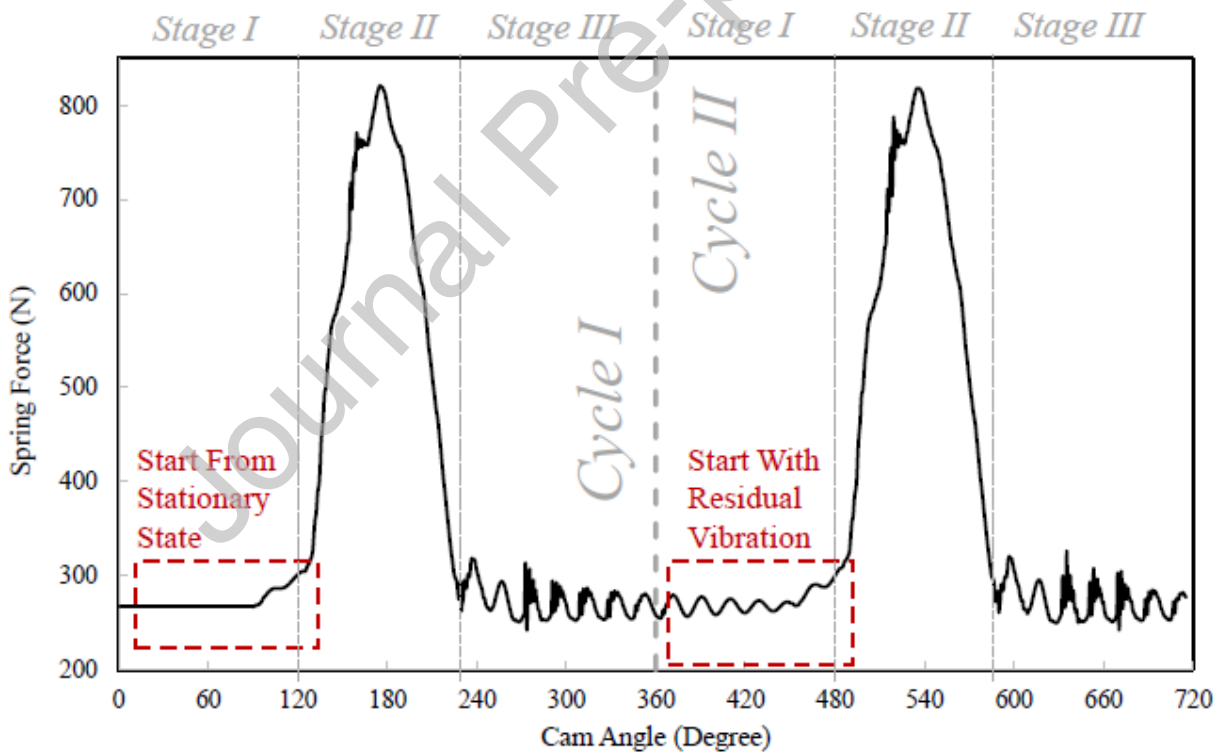


*Figure 7: A typical load and displacement relationship at engine speed: 4200-rpm*
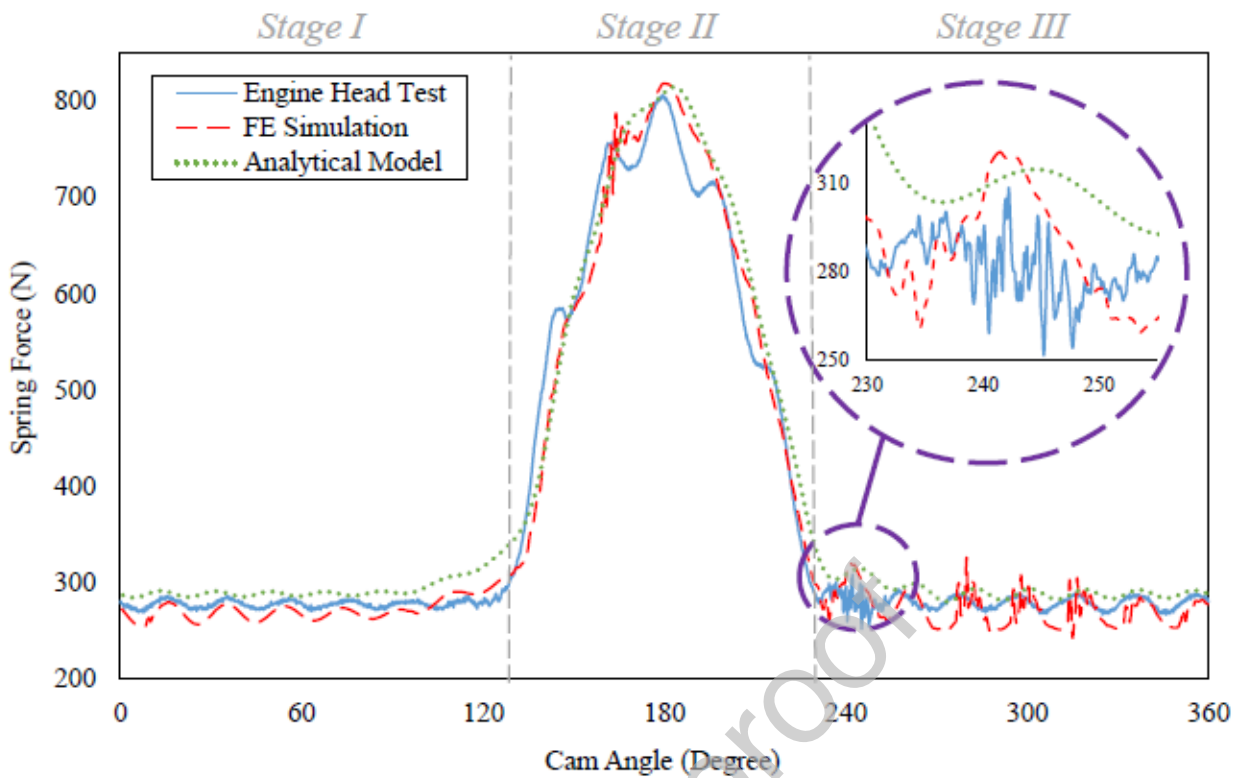
*Figure 8: Dynamic spring force curves of engine head test, FE simulation and analytical model at 4200-rpm engine speed.*
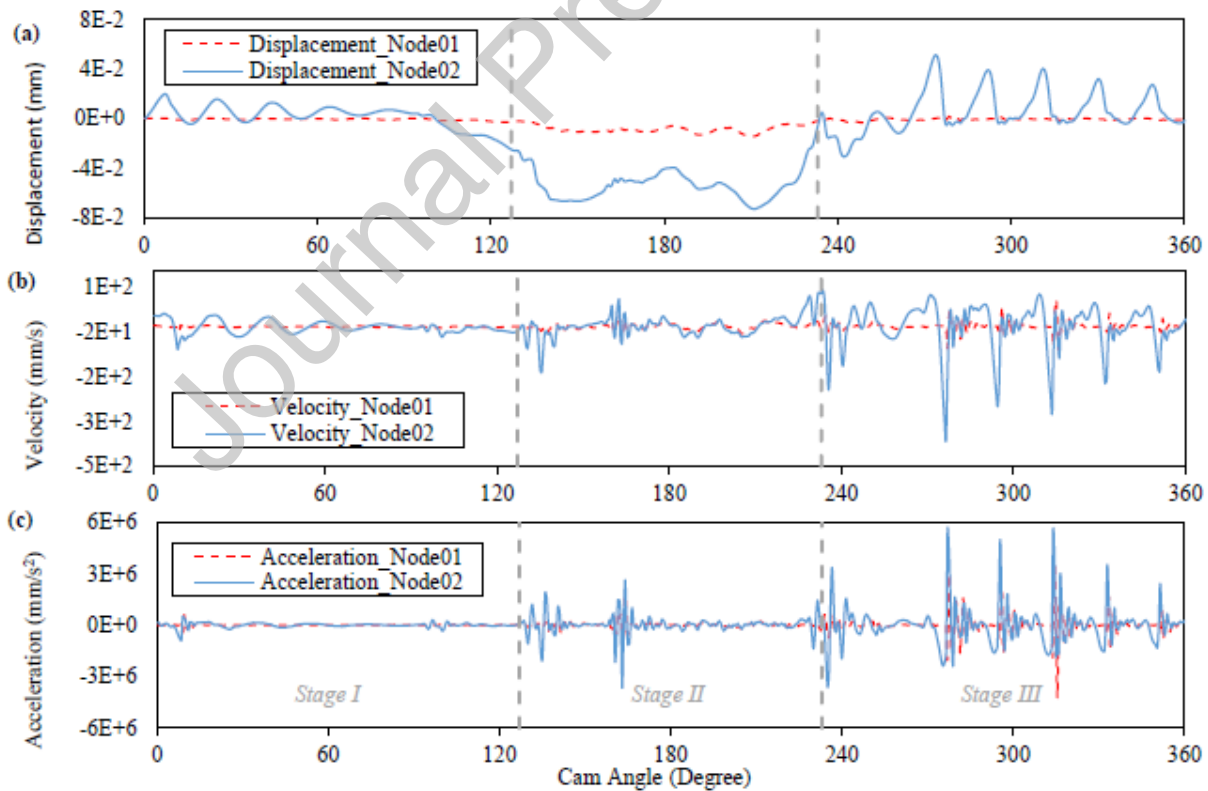


*Figure 9: (a). Displacements, (b). Velocities and (c). Accelerations of Node 01 and Node 02 along Z axis at 4200-rpm engine speed.*
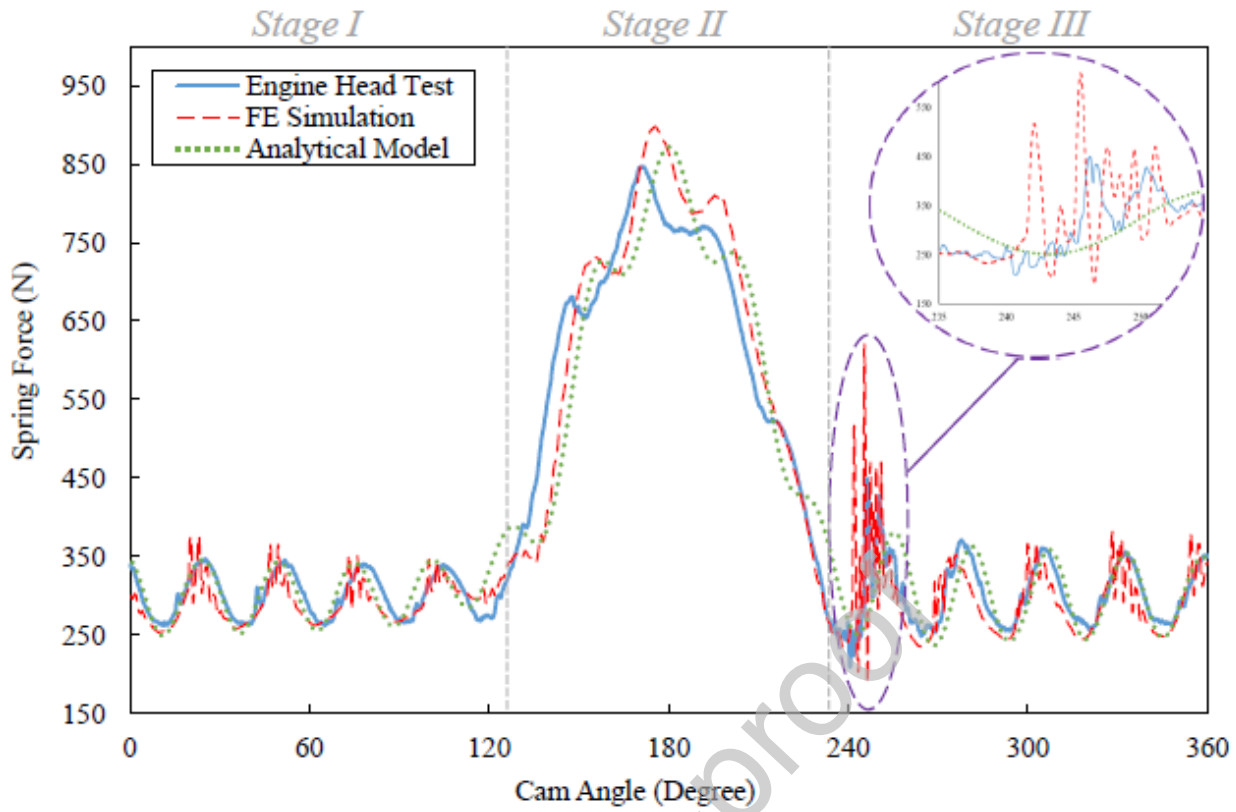
Figure 10: Dynamic spring force curves of engine head test, FE simulation and analytical model at 5600-rpm engine speed.
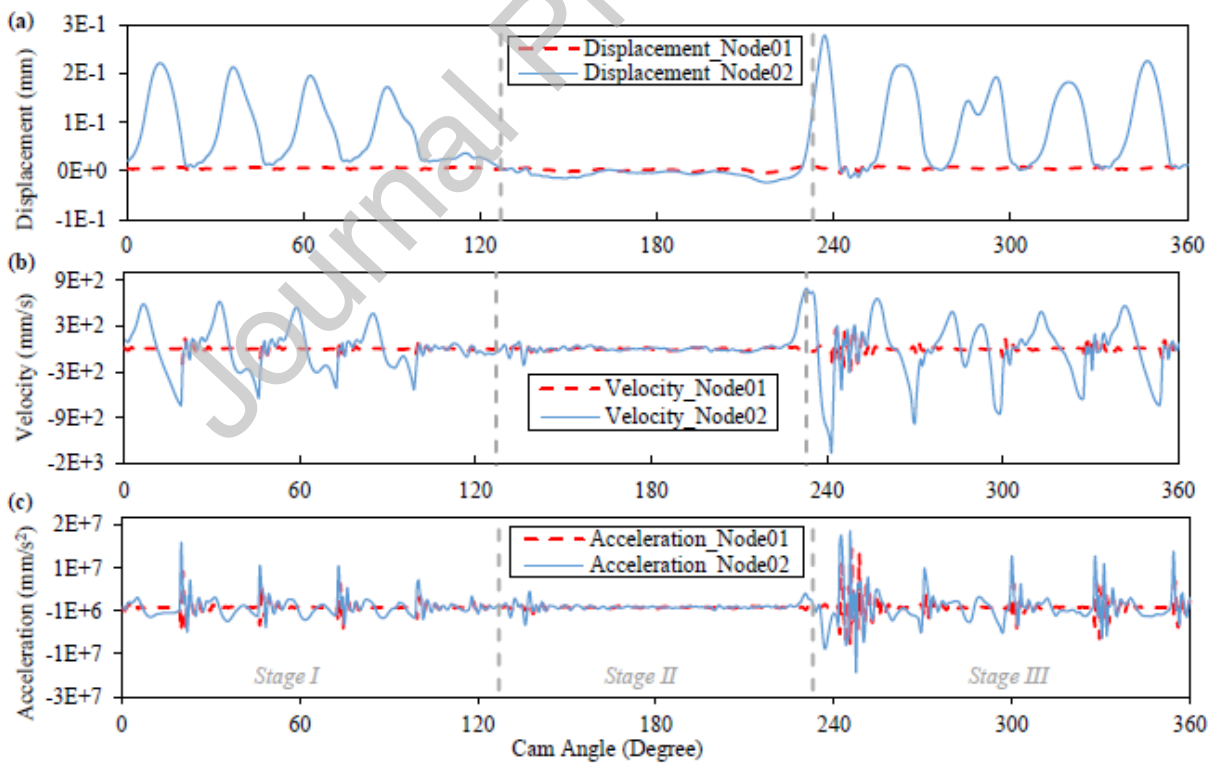


Figure 11: Acceleration, velocity and deformation curves of Node 01, 02 and 03 at 5600-rpm engine speed.
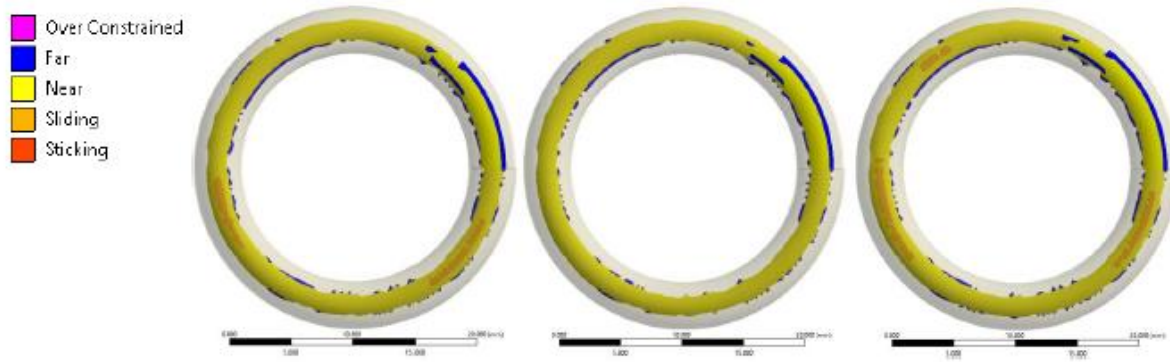
*Figure 12: Contact status of the coil 1 and coil 2 at (a). 240 degree, (b). 243.5 degree and (c). 245.5 degree under 5600-rpm engine speed.*
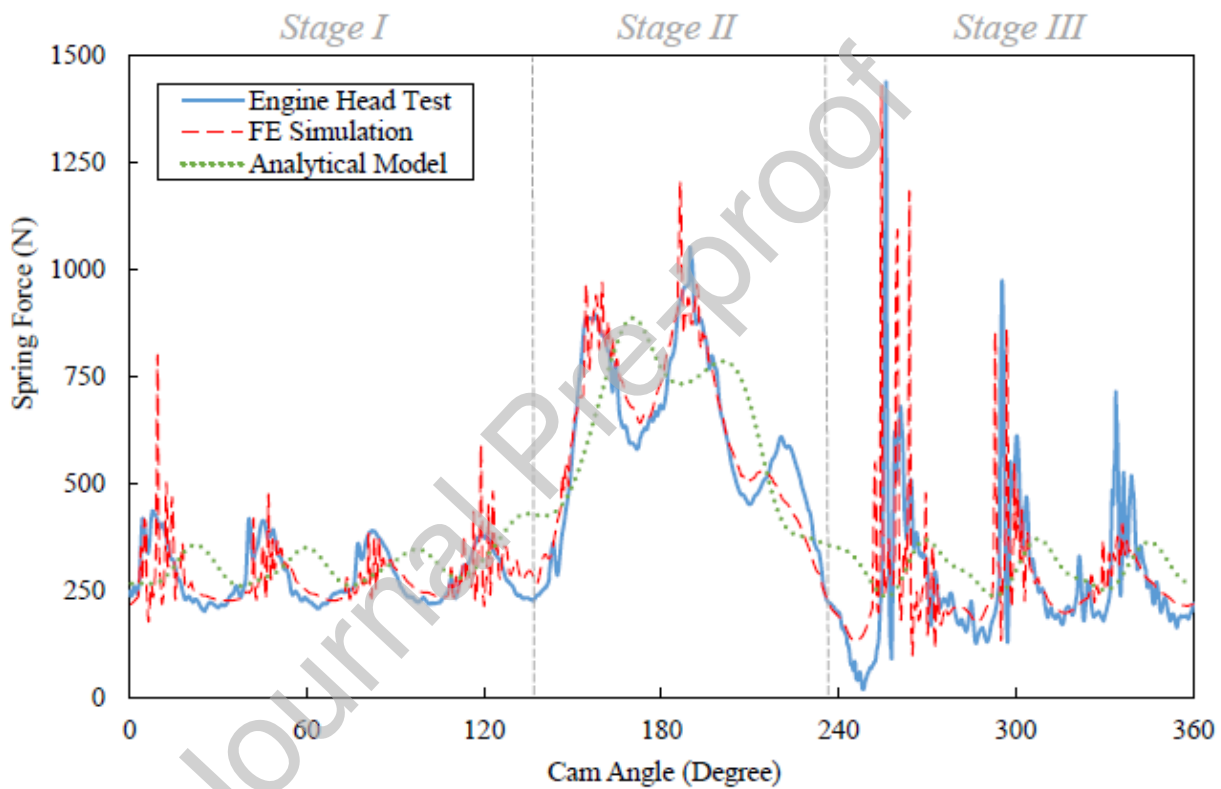


*Figure 13: Dynamic spring force curves of engine head test, FE simulation and analytical model at 8000-rpm engine speed.*
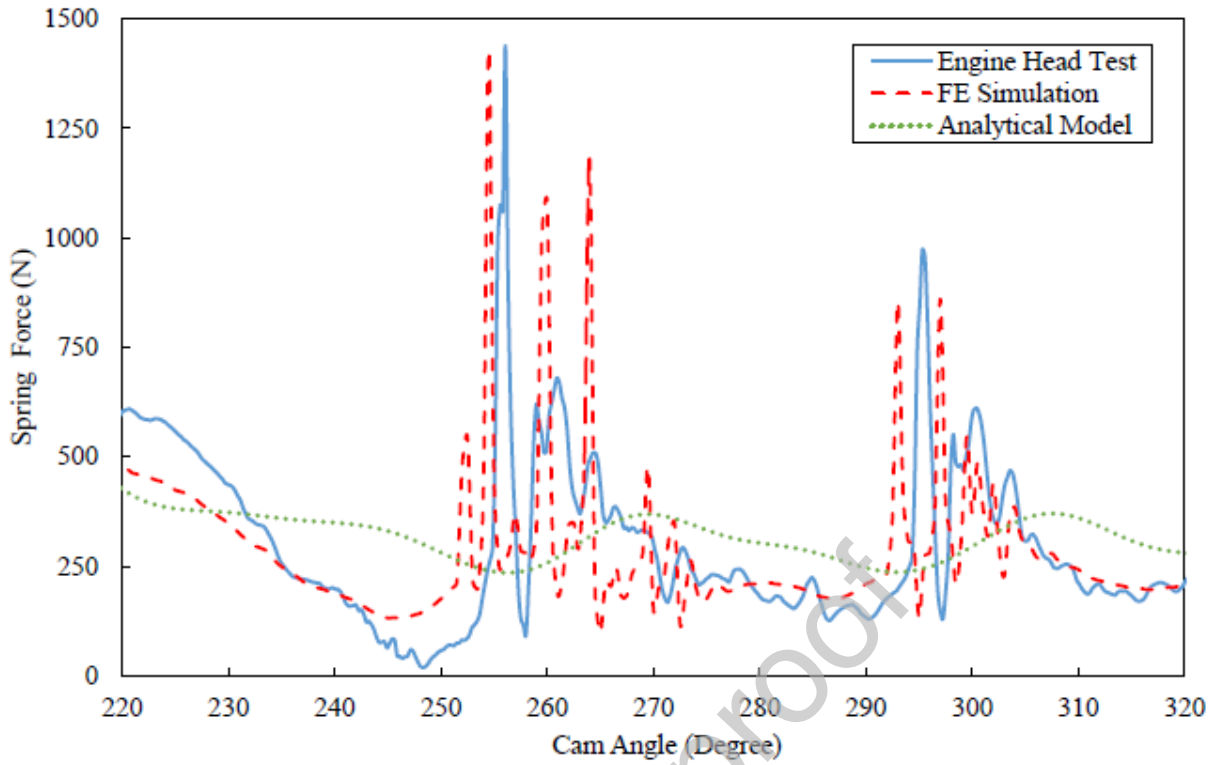
*Figure 14: Dynamic spring force curves of engine head test, FE simulation and analytical model at 8000-rpm engine speed between 220 degree and 320 degree cam angle.*
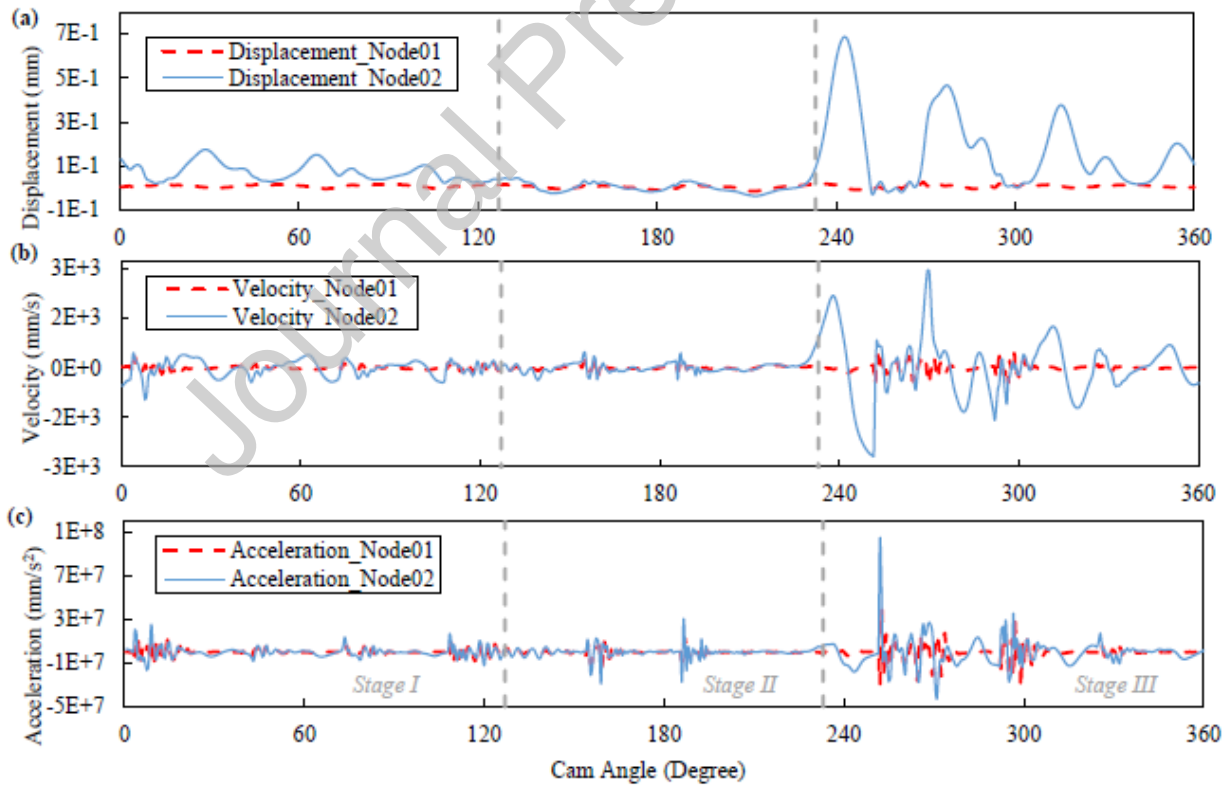


*Figure 15: Acceleration, velocity and deformation curves of Node 01, 02 and 03 at 8000-rpm engine speed.*
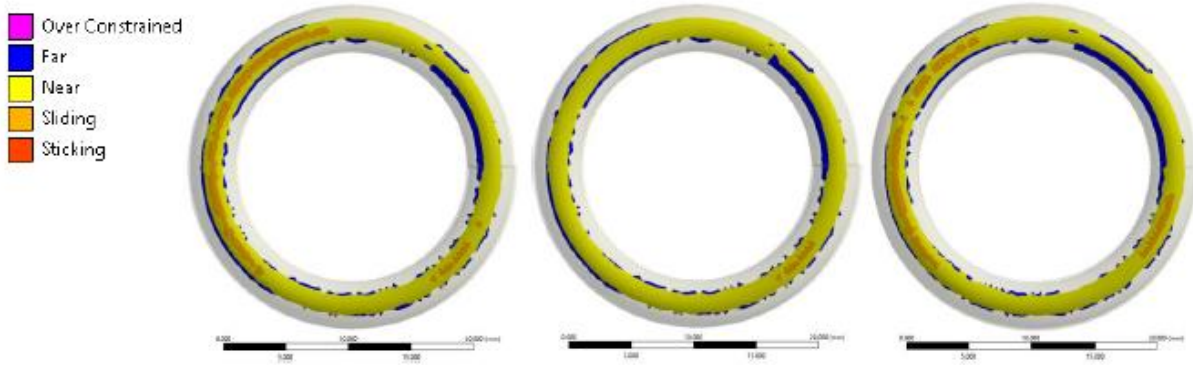
*Figure 16: Contact status of the coil 1 and coil 2 at (a). 253.5 degree, (b). 254.5 degree and (c). 255.5 degree under 8000-rpm engine speed.*

*Table 1: Frequencies of the first three modes of spring vibration*

| Mode of Vibration | First (01) | Second (02) | Third (03) |
|---|---|---|---|
| Frequency (Hz) | 630 | 1120 | 1639 |

*Table 2: The engine speeds, cam speeds, time of each analysis step and time of each sub-steps for the transient FE simulation*

| Engine Speed (RPM) | Cam Speed (RPM) | Time per analysis step (s) | Time per sub-step (s) |
|---|---|---|---|
| 4200 | 2100 | 3.97E-04 | 3.97E-05 |
| 5600 | 2800 | 2.98E-04 | 2.98E-05 |
| 8000 | 4000 | 2.08E-04 | 2.08E-05 |

**GRAPHICAL ABSTRACT**



Finite Element Modelling
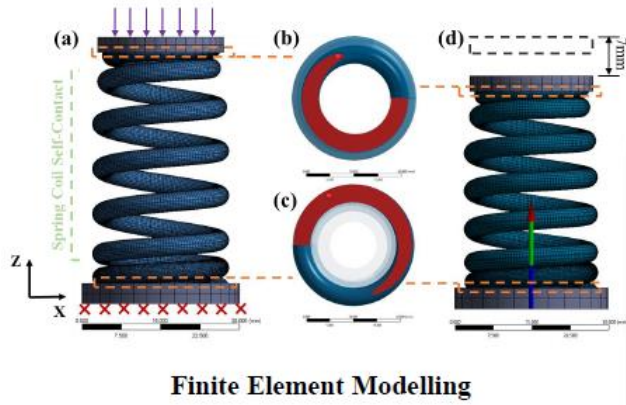


Dynamic Spring Force Response at High Engine Speeds